Available online at www.sciencedirect.com
SCIENCE DIRECT®
International Journal of Thermal Sciences 45 (2006) 405–418
International Journal of Thermal Sciences
www.elsevier.com/locate/ijts

Ice formation around a finned-tube heat exchanger for cold thermal energy storage

N. Kayansayan *, M. Ali Acar

Dokuz Eylül University, Department of Mechanical Engineering, Bornova 35100, Izmir, Turkey

Received 29 March 2004; received in revised form 8 March 2005; accepted 24 May 2005

Available online 5 August 2005

Abstract

This paper addresses a numerical and experimental investigation of a cold thermal energy storage system involving phase-change process dominated by heat conduction. The problem involves a fluid flowing inside a horizontal finned tube surrounded by a phase-change material (PCM). The objective of this paper is to predict the temperature distribution, the phase front distribution along the tube and to analyze the effect of fin density and size on the dynamic performance of the system. The problem is modeled as axisymmetric and two-dimensional, and a control volume computer code has been developed for the solution of the corresponding mathematical model. In the experimental arrangement of the tube configuration, two different fin diameters; $D_{\mathrm{fn}} = 2.7$ and 3.2 are considered and the fin density at each fin diameter is varied in the range of $N_{\mathrm{fn}} = 14$–31 fins·m^{-1}. For a particular geometry then the heat transfer fluid inlet temperature assumes values between $-10\,^{\circ}\mathrm{C}$ and $-20\,^{\circ}\mathrm{C}$, and the flow Peclet number is varied in the range from 14 350 to 200 900 accordingly. Comparison between the numerical predictions and the experimental data shows good agreement, even though some effects that are produced by heat transfer to the environment especially at high flow rates neglected in the model but unavoidable in the experiments. Finally, time-wise variation of energy stored by the system is evaluated through instant images of solidification fronts and the combined effect of fin parameters and the flow rate on energy storage is discussed.

Keywords: Heat transfer; Energy storage; Ice formation; Cold thermal energy; Finned tube; Numerical; Finite-volume; Phase change; Solidification; Experimental; Measurement

1. Introduction

Among the available techniques for storing cold thermal energy, the use of the solid–liquid phase change has attracted considerable attention in recent years. Use of this technique allows for a greater proportion of the base load to be utilised and hence the maximum generating capacity of cooling equipment can be reduced [1].

The present work is applicable to modelling of ice-on-finned-tube thermal storage systems where both the charge and the discharge of the phase-change material (PCM) (usually water) occur only from the flow inside the pipes. These systems typically consist of a large tank with a network of long tubes of relatively small diameter submerged in static water. A region of the PCM can be associated with each tube such that an outer symmetry (insulated) boundary approximation can be used. Due to small temperature difference between the tube outside surface and the PCM (less than 5 °C), natural convection is largely absent in these systems. Besides, the presence of vertical fins hampers the development of a buoyancy-driven flow. In fact, experimental observations by the authors indicate that nearly cylindrical layers of ice forming around the tube also signals the lack of convective currents within the PCM. During the phase-change process the interface of the two phase moves and its position is a priori unknown. This makes the mathematical model strongly non-linear. Further difficulties arise when the tube wall and the fins are at finite thicknesses. For all these reasons, no analytical solution for a particular simple case exist,

* Corresponding author. Tel.: +90 232 388 31 38; fax: +90 232 388 78 68.
E-mail address: nuri.kayansayan@deu.edu.tr (N. Kayansayan).

1290-0729/$ – see front matter
doi:10.1016/j.ijthermalsci.2005.05.009

Nomenclature

A	surface area of a control-volume	m^2
c_p	specific heat capacity at constant pressure	$J{\cdot}kg^{-1}{\cdot}K^{-1}$
C	non-dimensional heat capacity, $(\rho c_p)/(\rho c_p)_b$	
d	diameter	m
D	non-dimensional diameter, d/d_{pi}	
Fo	Fourier number, $\alpha_b t/d_{pi}^2$	
FVF	frozen volume fraction, dimensionless	
h	local heat-transfer coefficient	$W{\cdot}m^{-2}{\cdot}K^{-1}$
H	latent heat of freezing	$J{\cdot}kg^{-1}$
k	thermal conductivity	$W{\cdot}m^{-1}{\cdot}K^{-1}$
K	non-dimensional thermal conductivity k/k_b	
l	length of the finned tube	m
L	non-dimensional length l/d_{pi}	
$\dot{m}$	mass flow rate	$kg{\cdot}s^{-1}$
M	number of grids on the radial direction	
n_{fn}	number of fins on the heat exchanger	
N	number of grids on the axial direction	
N_{fn}	fin density	$fins{\cdot}m^{-1}$
Nu	local Nusselt number, hd_{pi}/k_b	
Pe	Peclet number, $4(\dot{m}c_p)_b/\pi d_{pi}k_b$	
Q	non-dimensional thermal energy stored, $q/\pi d_{pi}^3(\rho c_p)_b(T_{b,in}-T_{fr})$	
q	thermal energy stored	J
$\bar{q}$	thermal energy stored per meter of the finned surface	$J{\cdot}m^{-1}$
r	radial coordinate from the centre of the tube	m
R	non-dimensional length in r-direction, r/d_{pi}	
Re	Reynolds number, $4\dot{m}/\pi d_{pi}\mu$	
s	source term	$W{\cdot}m^{-3}$
Ste	Stefan number, $c_{pl}(T_{fr}-T_{b,in})/H$	
t	time	s
T	temperature	K
u	velocity component in axial direction	$m{\cdot}s^{-1}$
V	volume	m^3
w	fin spacing	m
x	axial distance from the pipe inlet	m
X	non-dimensional distance from the pipe inlet, x/d_{pi}	
y	fin thickness	m

Greek letters

α	thermal diffusivity	$m^2{\cdot}s^{-1}$
β	exponent	
δ	difference	
θ	non-dimensional temperature, $(T-T_{fr})/(T_{b,in}-T_{fr})$	
μ	dynamic viscosity	$kg{\cdot}m^{-1}{\cdot}s^{-1}$
ρ	density	$kg{\cdot}m^{-3}$
τ	solidification time of liquid between fins	s

Subscripts

b	bulk variable
c	cross section
ex	exit conditions, $x=l$
f	related to heat transfer fluid
fn	fin
fr	freezing
i	general axial grid
in	inlet conditions, $x=0$
init	initial conditions, $t=0$
j	general radial grid
j_{out}	radial grid adjacent to $r=r_{out}$
l	liquid
lh	latent heat
m	mean
out	outside wall surface, $r=r_{out}$
pi	pipe inside
po	pipe outside
s	solid
sh	sensible heat
sp	spacing
w	outer surface of the exchanger

Superscripts

n	general time level
$*$	refers to converted values

and for predictions of practical interest the use of numerical methods is required.

Numerous studies related to energy storage by liquid–solid phase change phenomenon have been published in the last decade. An excellent review on thermal energy storage in general and on cold thermal energy storage in particular is provided respectively by Zalba et al. [2] and by Saito [3]. Many researchers agree that adding lateral fins on the tube surface can offset the increase of thermal resistance between the cooling surface and the solid–liquid interface with the formation of ice. Lacroix [4] is the first who studied the melting of n-octadecane (n-$C_{18}H_{38}$) around a finned tube by the enthalpy based method. In his computational model, Lacroix [4] neglects the effect of the tube wall and the fin thickness on the thermal performance of the unit. Assuming uniform surface temperature, the local convective heat transfer coefficient inside the tube is determined in accord with the results of Graetz solution [5]. To validate his mathematical model, several melting experiments are conducted on a finned tube having the following configuration: $N_{fn}=12$ $fins{\cdot}m^{-1}$ with the fin-to-tube diameter ratio; $d_{fn}/d_{pi}=2.015$. Zhang and Faghri [6] numerically investigated the heat transfer enhancement of latent heat thermal energy storage systems by using internal fins and concluded that the performance of

systems designed for a heat transfer fluid with low thermal conductivity and operating at low flow rates may be increased by 15-percent. Zhang and Faghri [7] have also carried out similar studies for systems equipped with external radial finned tubes. In their analysis, contrary to Lacroix's mathematical model [4], the convection inside the tube is coupled with the melting of PCM and the tube wall temperature varies along the flow direction. Hence, the effect of tube wall thickness on molten volume fraction (MVF) is considered. However, without any rigorous definition of MVF and in the absence of experimental verification, Zhang and Faghri [7] conclude that increasing the height of the fins results with an increase in MVF of the exchanger. Lacroix and Benmadda [8] have numerically and experimentally studied the solid–liquid phase change from a finned vertical wall and have explained that increasing the number of fins will undoubtedly enhance the solidification rate. Ismail et al. [9] presents a numerical model for the solidification of phase change material around a radially finned tube with a constant wall temperature and perform numerical experiments to investigate the effects of the number of fins, fin material, fin thickness, and the tube wall temperature. In cold thermal energy storing systems, due to heat interaction between the heat transfer fluid and the PCM along the exchanger surface, the wall temperature is a function of both time and location, and could not be uniform. In fact, the present experimental observations reveal that, depending upon the flow rate and time, the surface temperature may vary in a range between 25% and 40% of its value at the inlet of the finned tube.

The lack of experimental modelling and the need for a computational algorithm to solve the freezing and the melting problem of a PCM surrounding a finned tube motivate this paper. This problem occurs in ice forming cold thermal energy storing systems. To verify the computational predictions and visualise experimentally the formation of ice, an experimental set-up is designed and developed. Besides the flow rate, the test apparatus is capable of altering the inlet temperature of the heat transfer fluid (HTF) as well as the finned tube geometry. In experiments, the fin diameter ratio spanned the range from 2.7 to 3.2, and the fin density from 14 fins·m^{-1} to 31 fins·m^{-1} accordingly. The objective of this paper is to device a computer code to predict the thermal performance, energy stored and phase front distributions along the finned tube and illustrate the accuracy of the code by experimental means. Besides the tube geometry, the analysis focuses on the roles of the Peclet, Fourier and Stefan numbers on the heat storage.

2. Experimental equipment and test procedure

A schematic diagram of experimental equipment is shown in Fig. 1. The flow system consists of a reservoir for the heat transfer fluid, a constant temperature circulating bath, a variable speed pump, a flow meter, a hydro-dynamic entry section, a main heat transfer test section, and the return piping for the HTF. The main heat transfer test section is composed of a container having a horizontal cross section of 50 cm × 57 cm, and a height of 42 cm and a finned tube being equidistant from the side walls of the container oriented at the mid-section. The container is filled with distilled water to a height of 40 cm. To record the images of solidifi-

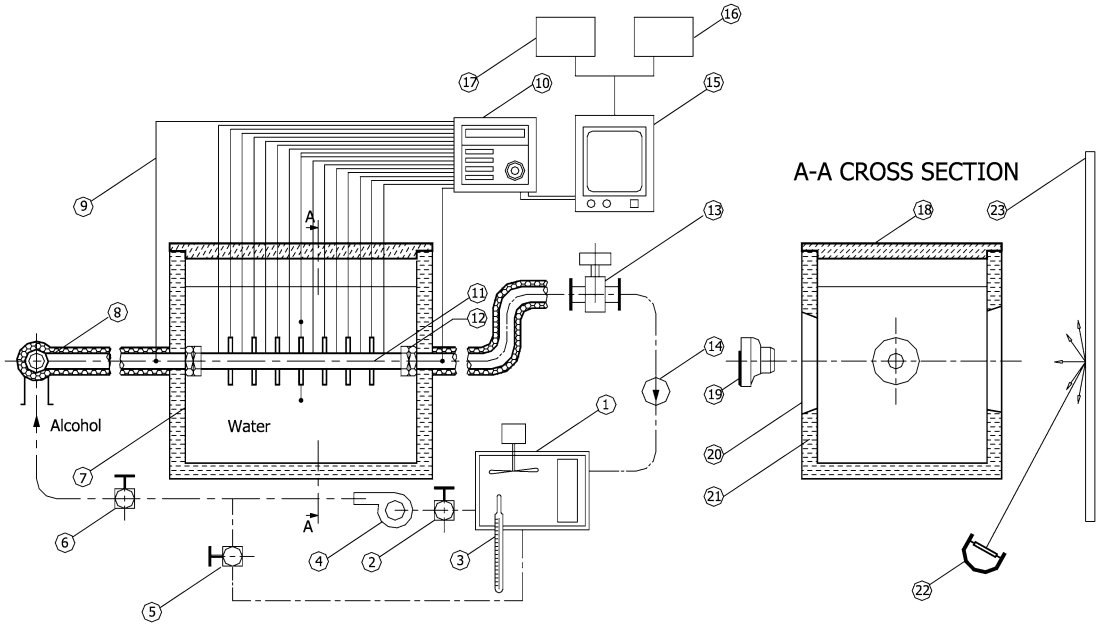

Fig. 1. Schematic diagram of the experimental equipment and apparatus: 1, Constant temperature bath; 2, main valve; 3, precision thermometer; 4, circulation pump; 5, recirculation valve; 6, flow adjustment valve; 7, test section; 8, alcohol recycling pipe; 9, thermocouple extension wire; 10, data logger; 11, finned tube; 12, fittings; 13, flow meter; 14, check valve; 15, PC computer; 16, monitor; 17, disc drive; 18, top cover; 19, digital camera; 20, view window; 21, insulation; 22, light source; 23, diffuse reflection screen.

cation around the finned tube, the front and back walls of the container are 10 mm thick Plexiglas. The two other lateral and the bottom surfaces are made out of 5 mm thick stainless steel sheet and the top surface is a 100 mm thick Styrofoam plate. To reduce the heat gain from the environment, the walls of the container are insulated with 100 mm thick Styrofoam layers. Two concentric and central openings having the dimensions of 25 cm by 18 cm is cut at each Styrofoam layer covering the Plexiglas walls. In taking an instant photography of solidification, these openings are necessary for the digital camera access and for the back screen lighting.

To eliminate any possible thermal contact resistance between the tube base and the fins, the finned tube for a particular configuration is a one-piece unit, and is produced by machining a solid bronze cylinder. The thermo-physical properties of the tube material having a laboratory based content of 87.2% Cu, 6.57% Sn, 4.13% Zn, and 1.97% Pb are determined by the available tables in Ref. [10]. All the finned tubes having the same length of 49.2 cm share the same inner and outer tube diameters of 20 mm and 30 mm respectively. In regard to fin-tube geometry, three different fin spacings of 14, 23, and 31 fins·m^{-1} are considered. Thus, for particular fin spacing, the fin diameters being at 54 mm and at 64 mm, a total of six distinct geometrical combinations are constructed and studied in the experiments. For the entire of experiments, the fin thickness is 3 mm. To attain fully developed flow conditions for the heat transfer fluid at the inlet of the test section, the hydrodynamic entry section is depicted to be 250-tube-diameter and the entire length of the experimental set-up is approximately 6.5 meters. To set the inlet temperature of heat transfer fluid to a desired value and control the flow rate, the apparatus contains several valves. Additionally, the entire piping is insulated with a 20 mm thick layer of foam rubber specially manufactured for refrigeration purposes.

The phase change material of the experiments is distillated water, and is charged into the system after a pre-cooling process to a temperature of 0.3 °C. The heat transfer fluid is 99% pure ethyl-alcohol, because it is chemically stable with very well known thermophysical properties from the literature [11]. Besides, using this fluid makes possible to study inlet temperatures as low as −20 °C in experiments. A Haake brand T model constant temperature bath with a sensitivity of ±0.1°C is used in providing the desired temperature to alcohol at the inlet of the test section. A variable speed pump circulates the alcohol through the flow system. To maintain steady flow of heat transfer fluid at predefined flow rates between 0.5 and 30 L·min^{-1} in experiments, the power supplied to the pump is first regulated and then fed to an electronic variance which in turn drives the pump. The alcohol supply is metered by a Schutte and Koerting type ASA glass tube variable area rotameter. The meter has a sensitivity of 0.5 L·min^{-1} per cm of the bob displacement and a maximum capacity of 30 L·min^{-1}. The meter is factory calibrated to be accurate within ±1% of the full range. The surface temperature of the finned tube is measured by copper-constant thermocouples (type T) of gage no. 24 calibrated by a precision thermometer. These thermocouples are distributed sequentially along the finned tube surface as one at the fin-tip and the other at mid-section of the base. Hence, depending upon the fin density of the exchanger under study, the number of thermocouples measuring the surface temperature may vary between 15 and 31. Two additional thermocouples measure the alcohol temperature at the inlet and outlet of the test section. Moreover, two thermocouples being vertically 20 cm apart in the test section detect any variation in temperature of the phase change material. The average temperature of alcohol in the reservoir is also checked by one additional thermocouple. A digital multimeter Hewlet–Packard HP34970A with an accuracy of ±0.04% of the reading is used to measure the electromotive force of each thermocouple. The data acquisition system is managed through a personal computer by means of an RS232 standard interface. The time is measured with the inner clock of the personal computer.

Prior to the experimentation, the uniformity of temperature in the container is assured through a mixing process. Hence the test section containing 110 L of still water at 0.3 °C with a temperature deviation within a range of ±0.1 °C, the alcohol at a predetermined flow rate is circulated through the system. In reducing the alcohol temperature to a desired value at the start of an experiment, the flow path first short-circuits the main test section. However, as the temperature reaches the specified inlet value, the alcohol is let abruptly into the test section by opening the inlet valve. Three different inlet temperatures of −10 °C, −15 °C, and −20 °C are studied. At each temperature however the alcohol flow rate is varied so that the flow Reynolds number ranged between 200 and 7000 in the experiments. Considering various combinations of the finned tube geometry, the alcohol inlet temperature and the flow rate, a total of 45 experimental runs are performed.

A typical experimental run lasts 150 minutes. The alcohol inlet and outlet, and the finned tube outer surface temperatures are measured and recorded at every fifteen seconds periods. However, the images of solidification profiles around the finned tube exchanger are taken at every 15 minutes. The Styrofoam lids at the front and at the back of Plexiglas surfaces are removed. The white light rays from a specially constructed halogen tube lamp incident upon a white screen reflect diffusely into the test section. Hence the necessary illumination for taking clear-cut picture of solidification field around the finned tube is provided. A digital camera, Fuji type MX600, is situated at the center and 20 cm away from the front opening of the test section, and is perpendicular to the approaching rays. The camera periodically takes the 24-bit color images of ice profiles at the size of 1280 × 1024 pixels with a resolution of 120 pixels per cm and transmits to the personal computer through a RS232 standard interface and data transfer software. Then these instantaneous color images are transformed to B&W intensity images. After applying special filtering techniques, bright

images that clearly indicate the boundaries of the ice formed around the finned tube are obtained. Considering the differences in pixel values between regions of solid and liquid phases, the edges of the solidified mass can be identified and thus the average thickness of ice at a particular cross section of the finned tube can be measured [12]. These measured quantities are then converted to the actual diameters of ice by linear proportioning with the fin diameter of that particular image. Finally, the volume of ice accumulated around the finned tube surface up to that instant of time becomes,

$$V_{\text{ice}}(t) = \frac{\pi}{4}\sum_i d^2_{\text{ice}_i}(t)\delta x_i - V_{\text{finned tube}} \tag{1}$$

Where $d_{\text{ice}_i}(t)$ is the instantaneous diameter at an axial location x_i on the finned tube and the volume occupied by the finned tube itself may be calculated as $V_{\text{finned tube}} = \pi[d^2_{\text{po}}l + (d^2_{\text{fn}} - d^2_{\text{po}})n_{\text{fn}}y]/4$. The axial increments, δx_i, assume identical values with the grid distribution of the numerical analysis. In studying the effect of fin density on ice profiles, an axial length corresponding to the distance between two fins of 14 fins·m^{-1} geometry is taken to be the reference length in experiments. Thus, at a particular experimental run, the diameters of ice-layer within this reference length are determined and substituted into Eq. (1). Moreover, for specified flow conditions and geometry, the sensible heat stored by the exchanger may be computed as,

$$q_{\text{sh}}(t) = \frac{\pi(\rho c_{\text{p}})_{\text{ice}}}{4}\sum_i (T_{\text{fr}} - T_{\text{w}_i})\left(\left(d^2_{\text{ice}_i} - d^2_{\text{po}}\right) + \frac{d^2_{\text{ice}_i}}{2\ln(d_{\text{ice}_i}/d_{\text{po}})}\left(1 - 2\ln\frac{d_{\text{ice}_i}}{d_{\text{po}}} - \left(\frac{d_{\text{po}}}{d_{\text{ice}_i}}\right)^2\right)\right)\delta x_i \tag{2}$$

In deriving this result, the temperature distribution in solid ice-layer is assumed to be a logarithmic function of radius. The experimental data also yield evaluating the latent heat part of the total energy stored by the exchanger as,

$$q_{\text{lh}}(t) = \left(\rho V(t)\right)_{\text{ice}} H \tag{3}$$

Hence the instant value of the total cold thermal energy stored by the system becomes,

$$q(t) = q_{\text{sh}}(t) + q_{\text{lh}}(t) \tag{4}$$

The uncertainties in the measured properties are estimated to be as in Table 1. With the uncertainties given in Table 1, and over the indicated ranges, the method of Kline and McClintock [13] is employed to evaluate the uncertainties of the experimental results. The maximum uncertainties are ±12.3% for the ice volume, and ±15.2% for the total energy stored by the system. For the flow Reynolds number, *Re*, the maximum uncertainty occurs at very low flow rates ($Re = 500$) and is determined to be ±25.4% of the reported value.

Table 1
Experimental uncertainties

Property	Uncertainty	Range
Alcohol flow rate	±0.5 L·min^{-1}	1.5–26.5 L·min^{-1}
Alcohol inlet and outlet temperature difference	±0.1 °C	0.5–3.5 °C
Finned tube surface temperature	±0.1 °C	−14 to −1.5 °C
Ice radius	±0.5 mm	22–51 mm
Finned tube dimensions	±1 mm	32–492 mm

3. Mathematical formulation and numerical solution

The physical system under investigation involves the radial and axial evolution of phase fronts along the outside of a horizontal finned tube. A pure substance with a freezing and melting temperature of T_{fr} is contained between the finned tube and an outer cylindrical wall of length l both of that are concentric. The thin outside wall is insulated and has a radius of r_{out}. The tube wall has inside and outside radii of r_{pi}, and r_{po}. There is a fluid of bulk temperature $T_{\text{b}}(x,t)$ and mass flow rate of $\dot{m}$ flowing inside the tube. The fluid enters the finned tube at a temperature of $T_{\text{b,in}}$ which is always less than T_{fr} and leaves the tube at $T_{\text{b,out}}(t)$. In formulating a mathematical model to represent this physical system, the system is divided into following three subsections: (i) the tube flow of heat transfer fluid, (ii) the finned tube, and (iii) the region occupied by the phase change material. Depending upon the region of the system under consideration, the related governing equations may be studied as follows.

Equations in the heat transfer fluid. Assuming that the axial conduction is negligible and the fully developed flow conditions exist at the tube inlet, the energy equation of the fluid can be expressed as,

$$k_{\text{b}}\frac{1}{r}\frac{\partial}{\partial r}\left(r\frac{\partial T_{\text{f}}}{\partial r}\right) = (\rho c_{\text{p}})_{\text{b}}\left(u\frac{\partial T_{\text{f}}}{\partial x} + \frac{\partial T_{\text{f}}}{\partial t}\right) \tag{5}$$

The initial and inlet conditions are,

$$T_{\text{f}} = T_{\text{init}}, \quad t = 0, \quad 0 \leqslant x \leqslant l$$
$$T_{\text{f}} = T_{\text{b,in}}, \quad x = 0, \quad t > 0 \tag{6}$$

Here, T_{f} represents the local temperature of the fluid and is a function of x, r, and t.

Integrating over the cross section of the tube and using the axisymmetric conditions at $r = 0$ reduces Eq. (5) to,

$$2\pi r_{\text{pi}}k_{\text{b}}\left(\frac{\partial T_{\text{f}}}{\partial r}\right)_{r=r_{\text{pi}}} = \pi r^2_{\text{pi}}(\rho c_{\text{p}})_{\text{b}}\frac{\partial T_{\text{m}}}{\partial t} + (\dot{m}c_{\text{p}})_{\text{b}}\frac{\partial T_{\text{b}}}{\partial x} \tag{7}$$

Where $\dot{m}$ is the mass flow rate, T_{b} and T_{m} represent accordingly the bulk and the mean temperatures of the heat transfer fluid. Note that T_{b} and T_{m} are defined as,

$$T_{\text{b}} = \frac{\int_0^{r_{\text{pi}}}(\rho c_{\text{p}})_{\text{b}}uT_{\text{f}}\,\mathrm{d}A_{\text{c}}}{\int_0^{r_{\text{pi}}}(\rho c_{\text{p}})_{\text{b}}u\,\mathrm{d}A_{\text{c}}} = \frac{\int_0^{r_{\text{pi}}}uT_{\text{f}}\,\mathrm{d}A_{\text{c}}}{u_{\text{m}}A_{\text{c}}} \tag{8}$$

$$T_{\text{m}} = \frac{\int_0^{r_{\text{pi}}}(\rho c_{\text{p}})_{\text{b}}T_{\text{f}}\,\mathrm{d}A_{\text{c}}}{\int_0^{r_{\text{pi}}}(\rho c_{\text{p}})_{\text{b}}\,\mathrm{d}A_{\text{c}}} = \frac{\int_0^{r_{\text{pi}}}T_{\text{f}}\,\mathrm{d}A_{\text{c}}}{A_{\text{c}}} \tag{9}$$

As stated by Eqs. (8) and (9), T_b is the bulk fluid temperature at a given cross section, A_c, and is defined in terms of the thermal energy transported with the bulk motion of the fluid as it moves through the cross section. The temperature T_m is the average temperature defined in terms of the lumped capacity or heat storage of the fluid. These two temperatures differ since the velocity is involved in T_b but is not in T_m. The thermal energy storage applications for the problem under investigation seldom consider sensible temperature differences of more than 10 °C below the tube wall temperature, T_{pi}. Thus the maximum possible difference between T_b and T_m is 7-percent with actual values much closer. Together with energy equation given by Eq. (7), the convective boundary condition between the fluid and the pipe wall may be expressed as,

$$-k_f\left(\frac{\partial T_f}{\partial r}\right)_{r=r_{pi}} = h_b(T_b - T_{pi}) = -k_p\left(\frac{\partial T_p}{\partial r}\right)_{r=r_{pi}} \tag{10}$$

Where T_{pi} represents the tube inside surface temperature and h_b is the forced convection heat transfer coefficient of the tube flow. Substituting Eq. (10) into (7) and replacing T_m with T_b yields the following:

$$2\pi r_{pi}h_b\big[T_{pi}(x,t) - T_b(x,t)\big] = \pi r_{pi}^2(\rho c_p)_b\frac{\partial T_b}{\partial t} + (\dot{m}c_p)_b\frac{\partial T_b}{\partial x} \tag{11}$$

The convection inside the tube is treated as a series of steady forced convection problems. For laminar and hydrodynamically fully developed flow with arbitrary varying temperature at the tube wall, the local value of heat transfer coefficient h_b in Eq. (11) may be determined as following [5],

$$(Nu_b)_i = \sum_{k=1}^{i}\delta T_k\sum_{n=0}^{\infty}G_n\exp\big[-\big(2\lambda_n^2/Pe\big)\big(X-(k-1)\delta X\big)\big] \times\left[2\sum_{k=1}^{i}\delta T_k\sum_{n=0}^{\infty}\frac{G_n}{\lambda_n^2} \times\exp\big[-\big(2\lambda_n^2/Pe\big)\big(X-(k-1)\delta X\big)\big]\right]^{-1} \tag{12}$$

where

$$\delta T_k = (T_{pi})_k - (T_{pi})_{k-1} \quad \text{and} \quad i = \text{int}\left(\frac{X}{\delta X}\right)+1 \tag{13}$$

The eigenvalues λ_n and the constants G_n in Eq. (12) may be found in Kays and Crawford [5]. For the transition and for the turbulent flow regimes of heat transfer fluid, including the thermally developing region, an average value of heat transfer coefficient h_b may be computed and substituted into Eq. (11) by using the empirical correlation of Gnielinski [14].

Equations in the finned tube and in the PCM. The mathematical modeling of these regions of the physical system is based on the following simplifications: (i) the thermophysical properties of each phase of PCM, and the finned tube material are independent of temperature, (ii) the PCM is homogeneous and isotropic, (iii) the phase change occurs over a range of temperatures from $(T_{fr} - \delta T)$ to $(T_{fr} + \delta T)$, (iv) the difference of density between liquid and solid does not create appreciable local motion of the liquid. The volume dilation due to ice formation between the fin spaces causes a radial outward motion of liquid PCM and the Reynolds number based on the time-wise averaged radial flow rate is evaluated as,

$$\overline{Re} = \frac{(\rho_l - \rho_{ice})d_{po}d_{fn}}{4\mu_l\tau}\left(1 - \frac{d_{po}^2}{d_{fn}^2}\right)$$

The experimental observations reveal that the magnitude of this Reynolds number varies in the range of 10^{-3} and 10^{-2} and the effect of such slow moving currents on heat transfer is certainly not traceable. Besides, the difference in temperatures between the liquid water and the ice front is always less than 0.5 °C and is not potentially sufficient to cause convective heat transfer from the liquid to the freezing interface [15]. Hence the heat transfer is controlled by conduction only and the energy equation for the finned tube and the PCM becomes,

$$\frac{\partial((\rho c_p)_* T^*)}{\partial t} = \frac{1}{r}\frac{\partial}{\partial r}\left(kr\frac{\partial T^*}{\partial r}\right) + \frac{\partial}{\partial x}\left(k\frac{\partial T^*}{\partial x}\right) - \frac{\partial s}{\partial t} \tag{14}$$

Where, $T^* = T - T_{fr}$ and depending upon the location in the solution domain the related parameters of Eq. (14) are defined in Table 2.

As shown in Fig. 2, for a computational domain; $r_{pi} \leqslant r \leqslant r_{out}$ and $0 \leqslant x \leqslant l$, the initial temperature of the system is the same as given by Eq. (6). However, the appropriate boundary conditions for this problem may be described as follows:

(1) Insulated surfaces include the outside wall, the inlet and the outlet planes of the exchanger as:

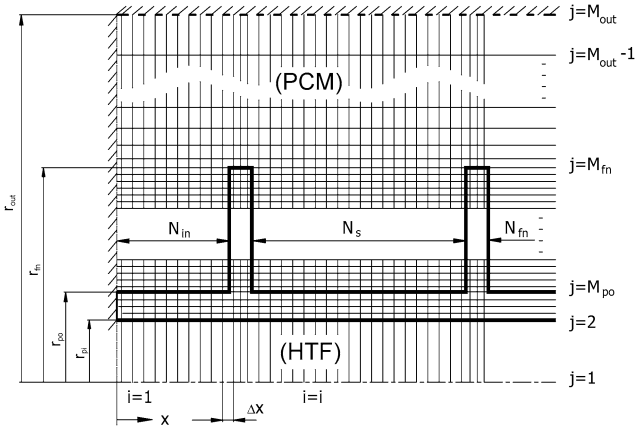

Fig. 2. Typical parameters of the flow geometry and discretization of the computational domain.

Table 2
Parameters of the finned tube and PCM as used in Eq. (14)

Parameter in Eq. (14)	Solution region	Restriction	Corresponding parameter
$(\rho c_p)_*$	Finned tube	none	$(\rho c_p)_p$
	PCM	$T^* < -\delta T$	$(\rho c_p)_s$
		$-\delta T^* \leqslant T^* \leqslant \delta T$	$\frac{1}{2}(\rho_s + \rho_l)(c_{pm} + \frac{H}{2\delta T})$
		$T^* > -\delta T$	$(\rho c_p)_l$
k	Finned tube	none	k_p
	PCM	$T^* < -\delta T$	k_s
		$-\delta T^* \leqslant T^* \leqslant \delta T$	$k_s + (k_l - k_s)\frac{T^* + \delta T}{2\delta T}$
		$T^* > -\delta T$	k_l
s	Finned tube	none	0
	PCM	$T^* < -\delta T$	$\rho_s c_{ps} \delta T$
		$-\delta T^* \leqslant T^* \leqslant \delta T$	$\frac{1}{2}(\rho_s + \rho_l)(c_{pm}\delta T + \frac{H}{2})$
		$T^* > -\delta T$	$\rho_s c_{ps}\delta T + \rho_l H$

$$\left(\frac{\partial T^*}{\partial r}\right)_{r=r_{out}} = 0 \quad \text{for } 0 \leqslant x \leqslant l \tag{15}$$

$$\left(\frac{\partial T^*}{\partial x}\right)_{x=0} = \left(\frac{\partial T^*}{\partial x}\right)_{x=l} = 0 \quad \text{for } r_{pi} \leqslant r \leqslant r_{out} \tag{16}$$

(2) Pipe outside surface:

$$\left.\begin{aligned} &-k_p\left(\frac{\partial T_p}{\partial r}\right)_{r=r_{po}} = -k\left(\frac{\partial T^*}{\partial r}\right)_{r=r_{po}} \\ &T_p(x, r_{po}, t) = T(x, r_{po}, t) \end{aligned}\right\} \tag{17}$$

$$\text{for } (2n-1)\frac{w}{2} + ny \leqslant x \leqslant (2n+1)\frac{w}{2} + ny$$

$$n = 1, 2, \ldots, n_{fn} - 1$$

(3) Surface at the fin tip:

$$\left.\begin{aligned} &-k_p\left(\frac{\partial T_p}{\partial r}\right)_{r=r_{fn}} = -k\left(\frac{\partial T^*}{\partial r}\right)_{r=r_{fn}} \\ &T_p(x, r_{fn}, t) = T(x, r_{fn}, t) \end{aligned}\right\} \tag{18}$$

$$\text{for } (2n-1)\frac{w}{2} \leqslant x \leqslant (2n-1)\frac{w}{2} + y$$

$$n = 1, 2, \ldots, n_{fn}$$

(4) Lateral fin surfaces:

$$\left.\begin{aligned} &-k_p\left(\frac{\partial T_p}{\partial r}\right)_{x=x^*} = -k\left(\frac{\partial T^*}{\partial r}\right)_{x=x^*} \\ &T_p(x^*, r, t) = T(x^*, r, t) \end{aligned}\right\} \tag{19}$$

$$\text{for } r_{po} \leqslant r \leqslant r_{fn}$$

Where, for the left surface of the fin, x^* is $(2n-1)\frac{w}{2} + (n-1)y$ and for the right, $(2n-1)\frac{w}{2} + ny$. In addition, the convective boundary condition at the tube inside surface that relates the fluid and the tube temperatures is given by Eq. (10).

Eqs. (11) and (14) together with the boundary conditions can be transformed into non-dimensional form by choosing the thermal diffusivity, the thermal conductivity, and the heat capacity of the heat transfer fluid, the inside diameter of the tube, and the freezing temperature of PCM as reference quantities. Then the significant dimensionless parameters of the problem are as follows,

$$\left.\begin{aligned} &L = \frac{l}{d_{pi}}, \quad \theta = \frac{T - T_{fr}}{T_{b,in} - T_{fr}}, \\ &Pe = \frac{4(\dot{m}c_p)_b}{\pi d_{pi} k_b}, \quad Fo = \frac{\alpha_b t}{d_{pi}^2} \\ &Ste = \frac{c_{pl}(T_{fr} - T_{b,in})}{H}, \quad K = \frac{k}{k_b}, \quad C = \frac{\rho c_p}{(\rho c_p)_b} \end{aligned}\right\} \tag{20}$$

The resulting non-dimensional equations as well as the initial and the boundary conditions are discretised by employing the control-volume based finite difference method and by implicit formulation for the temperature equations [16]. Referring to Fig. 2 for grid distribution in the computational domain, fine grid spacing was applied to a region between r_{pi} and r_{fn} where high temperature gradients were expected. However, the grid spacing need not necessarily be uniform in size for the entire solution domain. Starting from the fin tip, the increment size of the grids is taken to be 4% greater than the previous size. A total of 114 nodes are allocated in radial direction and 60 of which are in a region between r_{fn} and r_{out}. In the axial direction, the number of nodes for one fin spacing is 24 and kept constant for all configurations. Hence the total number of nodes in the axial direction increases as the fin number increases and varies between 168 and 360 nodes in the analysis.

Computational algorithm. Beginning with the liquid phase of PCM, all temperatures are initialized to θ_{init}. At time $Fo = 0$, the inlet temperature of the heat transfer fluid is set to $\theta_{b,in} = 1$. The strongly implicit solver that requires considerably less storage and computational time per iteration than the other available iterative solution algorithms [17] is implemented in solving the set of simultaneous equations assembled for the unknown temperatures of the domain. Due to need of accurate calculation of the energy stored by the exchanger especially at initial time steps, the increments in

Fo have to be kept small. Hence the value of δFo at a particular time interval is determined with respect to the frozen volume fraction (*FVF*) of the exchanger which is defined as,

$$FVF(t)\% = \frac{V_{\text{ice}}(t)}{V^*} \times 100$$
$$V^* = \frac{\pi}{4} d_{\text{fn}}^2 l - V_{\text{finned tube}} \tag{21}$$

Thus, δFo assumes two different values in the numerical analysis. For values of FVF less than 5-percent, the time step is assumed to be 0.001, otherwise $\delta Fo = 0.003$. Numerical experimentation showed that these choices produced results that were independent of segment size both in radial and axial directions and in time step. At a particular time level of n, convergence in temperature is declared at the $(m+1)$th iteration when the following condition is satisfied at all nodes of the computational domain.

$$\left|\theta_{m+1}^n(i,j) - \theta_m^n(i,j)\right| \leqslant 10^{-\beta}$$
$$i = 1, \ldots, N_t \text{ and } j = 1, \ldots, M_{\text{out}} \tag{22}$$

The value of β in Eq. (22) is determined with respect to the overall energy balance of the exchanger. The increase in enthalpy of the heat transfer fluid for a time step of δt^n must be equal to the total energy supplied on the inner surface of the exchanger tube as follows,

$$\left(\frac{Pe\,\delta Fo^n}{4}\right)\left[\theta^n(1,1) - \theta^n(N_t,1)\right]$$
$$= 2\sum_{j=1}^{N}\sum_{i=1}^{M} R_j C(i,j)\left(\theta^n(i,j) - \theta^{n-1}(i,j)\right)\delta R_j \delta X_i$$
$$+ C_{\text{s}}\left(\frac{V^*}{\pi d_{\text{pi}}^3}\right)\left(\frac{FVF^n - FVF^{n-1}}{Ste_{\text{s}}}\right) \tag{23}$$

The left-hand side of Eq. (23) represents the total energy removed from the exchanger by the heat transfer fluid for a time step of δt^n. Including the energy change of the exchanger tube-material, the right-hand side is the total cold thermal energy stored (sensible + latent). Hence, in providing a solution to the temperature field, the exponent β in Eq. (22) is altered in a range; $(5 \leqslant \beta \leqslant 7)$ so that the deviation between the energy flow out of the system and the cold thermal energy stored by the system is less than 5-percent. Computations are conducted on a Pentium IV personal computer and depending upon the flow rate, the CPU time varied in a range between 2-hour and 16-hour for the simulation of a 2.5-hour freezing problem.

4. Numerical code validation

When the heat transfer fluid inlets the exchanger at a temperature above the melting point of the phase change material, then the present code analyzes the melting of a PCM for which extensive numerical results are provided in literature [4,7]. For such a case, a comparison exercise between numerical results may be arranged in order to evaluate the reliability of the present approach. In simulating Lacroix's mathematical model [4], the tube wall possesses certain thickness and no lump analysis is applied to the fins. Even though the fins are subdivided by the grid lines, to attain a uniform distribution of temperature across the thickness, they are assumed to be very thin in the present comparison process. The related geometric and flow parameters are the same as those applied by Lacroix [4], who chose water as the working fluid, and *n*-octadecane (n-$C_{18}H_{38}$) as the PCM. In validation exercise, the comparison is carried out for a finned tube equipped with 12 fins, and the working fluid assumes Peclet numbers of 75.4, 754, and 7540 respectively. In Fig. 3, the effect of flow rate on the molten volume fraction (MVF) and on the exit temperature of the heat transfer fluid is compared with the results of Lacroix [4]. Owing to the local heat capacitance of the tube wall, the tube material absorbs some portion of the released energy. Especially at low flow rates ($Pe = 75.4$), due to fundamental differences in mathematical modeling, the results do not appear to be fully consistent. The non-uniformity in the wall temperature strongly affects the distribution of MVF. As shown in Fig. 3, the diminished values of MVF data is in accord with the time wise variation of the exit temperature of the heat trans-

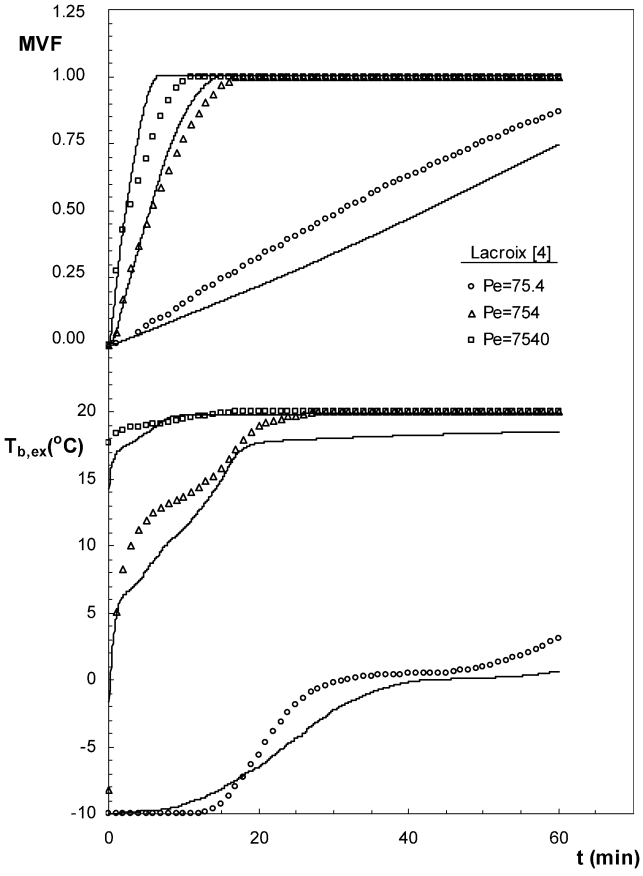

Fig. 3. Validation test: numerical comparison of heat transfer fluid exit temperatures and (*MVF*) values with Lacroix [4] (lines: present results, symbols: Lacroix's results).

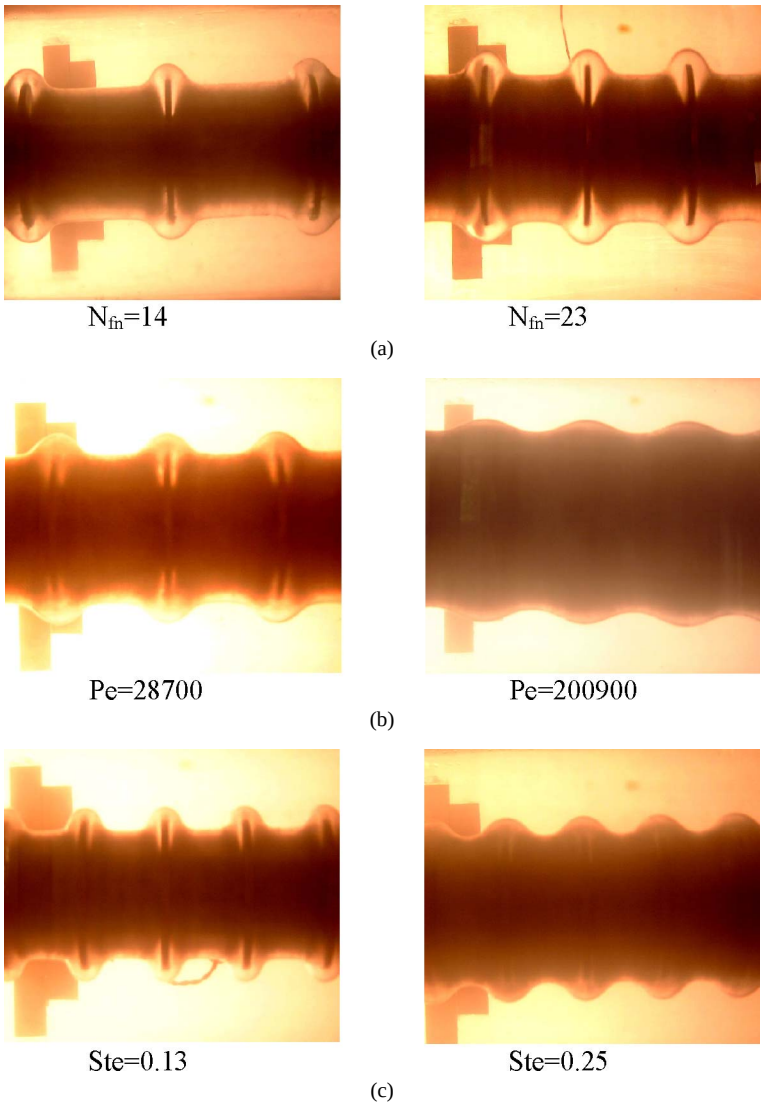

Fig. 4. Images of phase fronts at mid-section of the finned tube ((a) $D_{fn} = 3.2$, $Fo = 1.83$, $Pe = 14\,350$, $Ste = 0.19$; (b) $D_{fn} = 2.7$, $N_{fn} = 23$, $Fo = 1.22$, $Ste = 0.19$; (c) $D_{fn} = 2.7$, $N_{fn} = 31$, $Fo = 0.61$, $Pe = 143\,500$).

fer fluid as depicted by the lower curves of the same figure. As the flow rate increases, however, the discrepancy due to wall heat capacitance and wall temperature becomes negligible and the agreement between the two numerical results becomes satisfactory.

5. Results and discussion

Having demonstrated the numerical validity of the code by comparing with the results of Lacroix [4], the physical validity of the mathematical model may be studied by comparison of predictions with the experimental data. Fig. 4 presents the photographic images of solidification fronts at the indicated values of fin densities (Fig. 4(a)), the flow rates (Fig. 4(b)), and the Stefan numbers (Fig. 4(c)). The actual diameters of ice determined by using such images are utilized in evidencing the validity of numerical predictions. In fact, Figs. 5–7 display the axial evolution of phase fronts at various flow and geometric parameters. In each figure, the Fourier number is kept constant at 1.22. For all tests reported in these figures, the presence of interface separating the liquid zone from the solid is clearly evidenced. Then the experimental evaluation of the local radius of ice on the images is accomplished by generating uniform grids at $\delta x = 0.5$ mm apart from each other and extending one fin spacing to the left and to the right from the mid-section of the exchanger. Symmetry in experimental profiles is checked for any possible effect of convection currents. The profiles being straight-sided with a thicket of discrete crystals on the finned surface confirm the decision to neglect all phenomena but the conduction. Hence the experimental results on solidification fronts are compared well with the numerical data. The effect of fin density on solidification profiles is illustrated in Fig. 5. An increase in solidification rate due to fin density is noted and ratified by the relative increase in exit

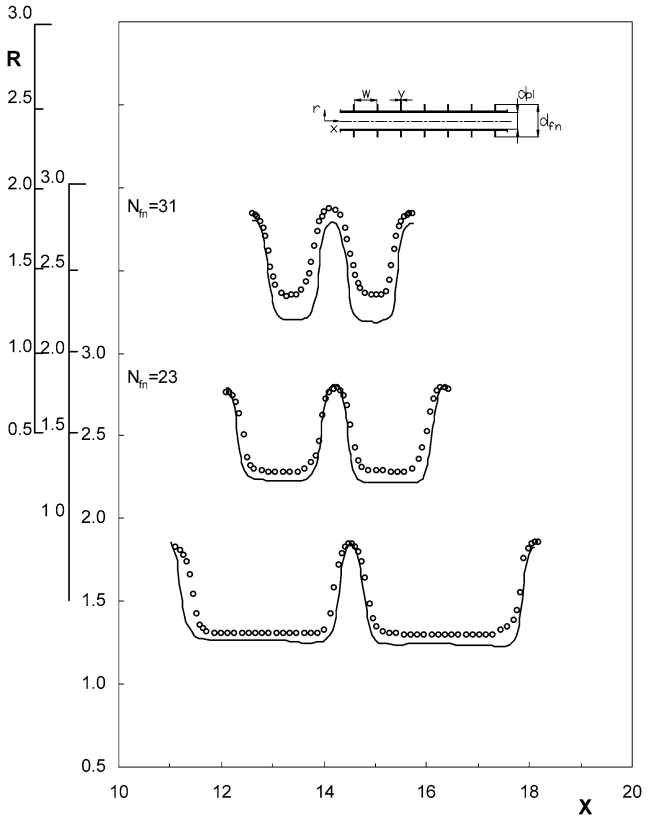

Fig. 5. Effect of fin density on solidification and comparison between computed (lines) and measured (symbols) profiles of phase fronts for tests: $Pe = 28\,700$; $Ste = 0.19$; $Fo = 1.22$; $D_{\mathrm{fn}} = 3.2$.

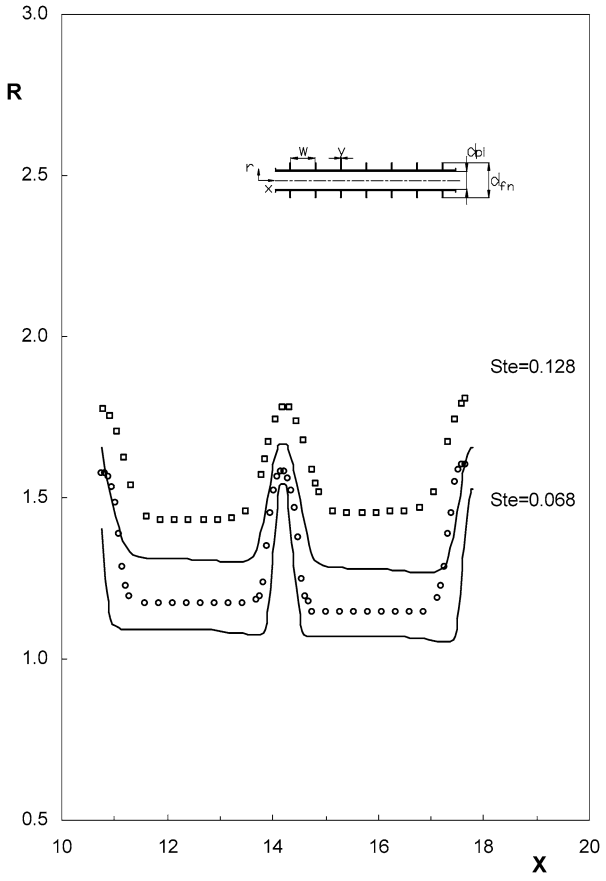

Fig. 6. Effect of fluid inlet temperature on solidification and comparison between computed (lines) and measured (symbols) profiles of phase fronts for tests: $Pe = 14\,350$; $Fo = 1.22$; $N_{\mathrm{fn}} = 14$; $D_{\mathrm{fn}} = 2.7$.

temperature of the heat transfer fluid as the fin density increases at a particular flow rate. The effect of fin density on solidification rate is further discussed in the following sections as the FVF characteristics of the exchanger exhibited. As depicted in Fig. 6, the effect of Stefan number on solidification rate is demonstrated by reducing the inlet temperature of alcohol from $-10\,^{\circ}\mathrm{C}$ to $-20\,^{\circ}\mathrm{C}$, and on the average 15-percent of increase in phase-change rate is noticed. Fig. 7 reveals that increase in flow Peclet number also causes an increase in the amount of accumulated ice. In Fig. 7 even though the numerical model yields trends of phase fronts totally similar to those experimentally determined, a maximum of 12% shift in results is noticed for high flow rates ($Pe = 143\,500$). One of the essential factors responsible for such a discrepancy between measured and predicted interface positions is the experimental difficulty in minimising the heat gains from the surroundings at high flow rates. The faster advance of solidification front at high flow rates of HTF affects the temperature gradients in liquid PCM and causes an increase in heat gains. Since the numerical model assumes adiabatic boundary at the lateral walls of the test section, the code tends to predict larger values of radius at the solid–liquid interface than the experimental counterpart at high flow rates.

Fig. 8 exemplifies the variation of the non-dimensional wall temperature on the outer tube surface for two different Fourier numbers. All curves in this figure are obtained for the same flow rate ($Pe = 28\,700$) and the fin density ($N_{\mathrm{fn}} = 14$) but the top curves are for a fin diameter of 3.2 and the bottom ones are for $D_{\mathrm{fn}} = 2.7$. Experimental results are the output signals of the thermocouples located at midsections between consequent fins. In Fig. 8, no appreciable effect of fin diameter on wall temperature distribution is noticed at low Fourier numbers ($Fo = 0.61$) and almost similar profiles of surface temperature distribution are recorded. At high Fourier numbers ($Fo = 2.44$), however, increase in solidification rate due to increase in fin diameter is better felt by the finned surface and more ice is accumulated for the same time interval of operation. Hence, at large time intervals, the ice layer on the finned surface being much thicker for larger fin diameter causes a higher thermal resistance that in turn reduces the actual tube wall temperature. This effect exhibits itself as an increase in non-dimensional wall temperature distribution in Fig. 8.

In accord with Eq. (25), the instantaneous value of FVF is evaluated from the solid–liquid interface by a numerical integration of the ice volume accumulated up to that instant of time, t. A comparison of the experimental data with the predicted FVFs is shown in Fig. 9. These results are for two different fin densities of $N_{\mathrm{fn}} = 14$, and 31 re-

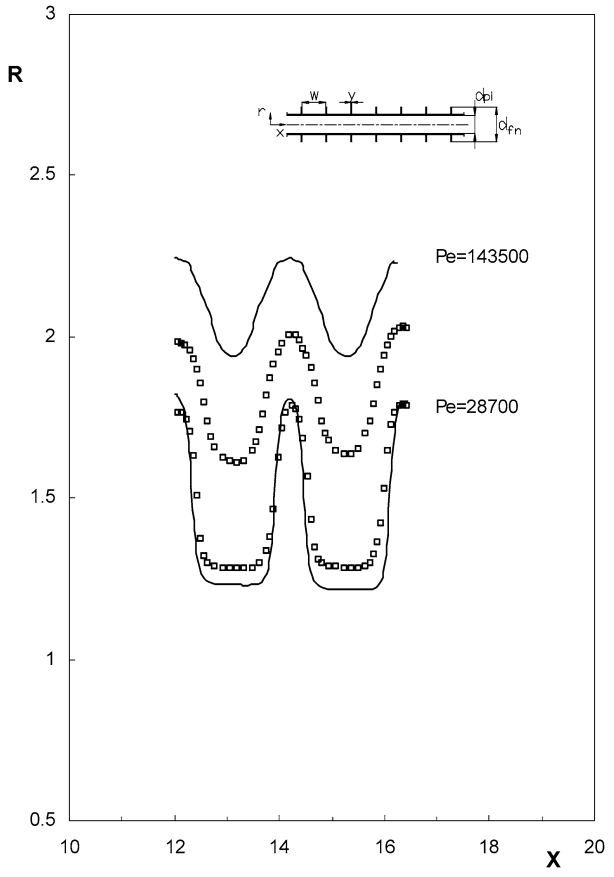

Fig. 7. Effect of flow Peclet number on solidification and comparison between computed (lines) and measured (symbols) profiles of phase fronts for tests: $Ste = 0.19$; $Fo = 1.22$; $N_{fn} = 23$; $D_{fn} = 3.2$.

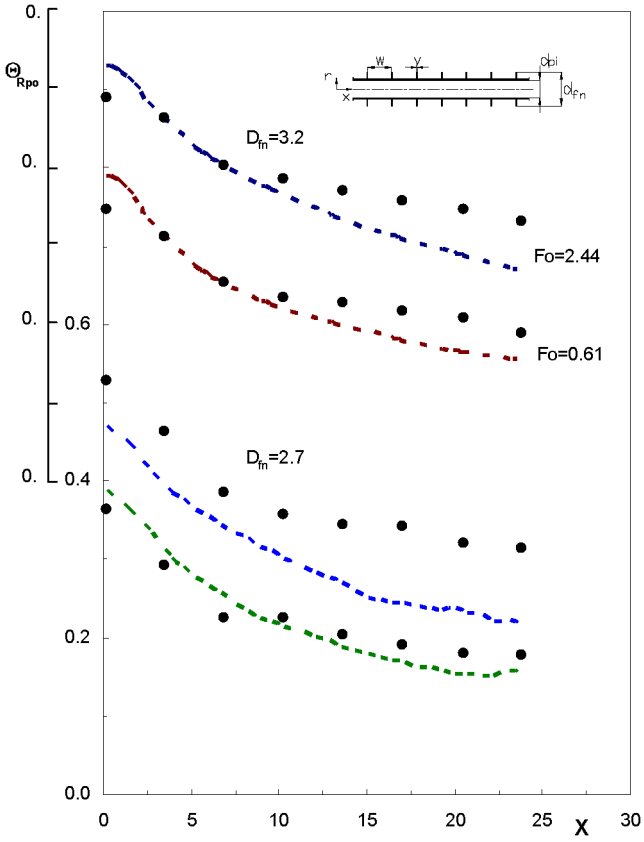

Fig. 8. Comparison between computed (dotted lines) and measured (symbols) tube outer surface temperature distributions at two different fin-diameter-ratio and Fourier numbers for tests: $Pe = 28\,700$; $Ste = 0.19$; $N_{fn} = 14$.

spectively. The fin diameter ($D_{fn} = 3.2$) and the HTF inlet temperature ($Ste = 0.19$) are kept constant but two different flow rates ($Pe = 28\,700$, $143\,500$) are considered for these particular experiments. Despite a maximum discrepancy of 6-percent taking place at high flow rates and high Fourier numbers, the agreement between measured and predicted FVF values is satisfactory. On these curves, the numerical value of the derivative; dFVF/dFo, determined at a particular Fo number is a measure of the average solidification rate of the exchanger at that particular instant. Hence, it is clear from Fig. 9 that as the number of fins increases so does the overall freezing rate. Especially, at the initial period of freezing ($Fo \to 0$), the difference in freezing rate is distinct. As time advances, however, this difference gets smaller and approaches to a limiting value. As expected, the effect of fin density on freezing rate is better felt at high flow rates. For instance, at $Fo = 2.0$, increase in frozen volume fraction due to change in fin density from $N_{fn} = 14$ to 31 is 51.6-percent at $Pe = 143\,500$, however, this increase for the same change in fin density is reduced to 12.9-percent at $Pe = 28\,700$.

The results on energy behaviour of this phase-change system have also been compared. In energy analysis, to illustrate the validity of the present mathematical model, in addition to the fin density and the fin diameter, the flow conditions have also been altered. For two cases of the tube geometry characterised by ($N_{fn} = 14$, $D_{fn} = 2.7$), and ($N_{fn} = 263$, $D_{fn} = 3.2$), and the inlet and flow conditions respectively at $Ste = 0.19$, $Pe = 14\,350$, $28\,700$, and $57\,400$, the trends of total cold thermal energy as a function of the Fourier number are presented in Fig. 10. In this figure, Q represents the dimensionless instant value of the total cold energy stored in the system and defined as,

$$Q(Fo, Pe, Ste, N_{fn}, D_{fn}) = \frac{q(t)}{\pi d_{pi}^3 (\rho c_p)_b (T_{b,in} - T_{fr})} \qquad (28)$$

In experiments, $q(t)$ is determined by Eq. (4) for which the required ice diameters, $d_{ice_i}(t)$, should be the results of snapshots presenting the complete ice profile formed along the tube surface. However, the aforementioned experimental conditions and the present photography techniques do not yield any solution to this desire. In accord with the wall temperature distributions of the exchanger, the experimental observations reveal that the ice formed at the inlet section is thicker than the ice layer formed at the exit of the tube. Depending upon the HTF inlet temperature, the flow conditions, and the time, the difference in thicknesses may vary. At low flow rates, since the heat transfer coefficient, h_b, is a strong function of length, x, a maximum of 27-percent deviation in ice diameter along the flow direction is measured

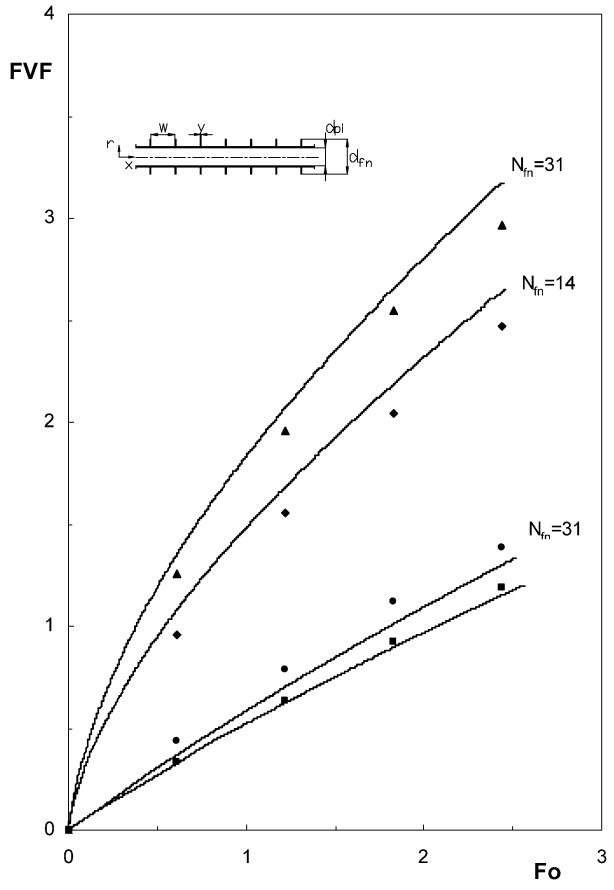

Fig. 9. Comparison of computed (lines) and experimental (symbols) time-wise variation of (*FVF*) results for tests: $Ste = 0.19$; $D_{\mathrm{fn}} = 3.2$, at flow rates of $Pe = 28\,700$ (lower curves) and 143 500 (upper curves).

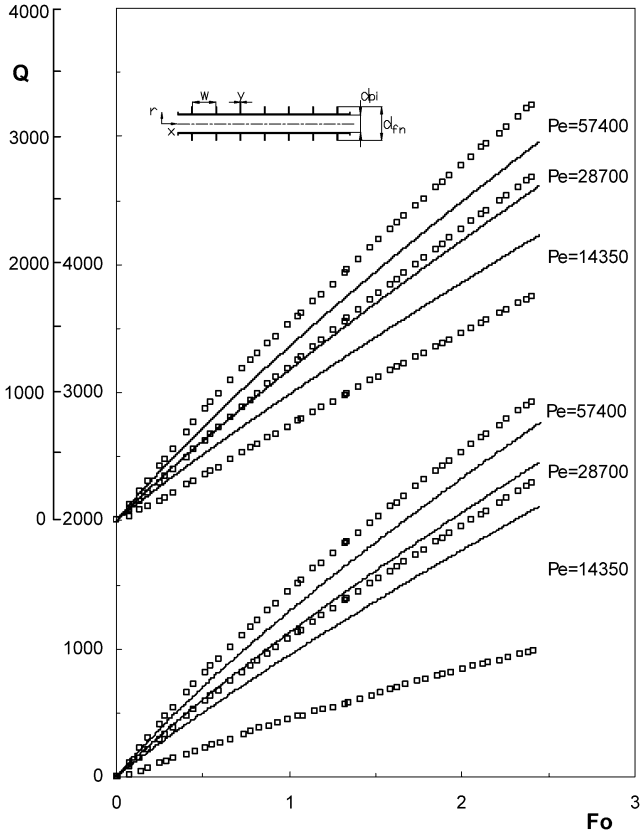

Fig. 10. Comparison of computed (lines) and experimental (symbols) time-wise variation of the total thermal energy stored in the system for tests at $Ste = 0.19$ with the exchanger geometry specified as: $N_{\mathrm{fn}} = 14$; $D_{\mathrm{fn}} = 2.7$ (lower curves), and $N_{\mathrm{fn}} = 23$; $D_{\mathrm{fn}} = 3.2$ (upper curves).

after a 21/2-hour of test run. Hence, in estimating the total volume of ice, the ice-layer diameters measured at the mid-section and extending only about three-fin spacing are linearly extrapolated to the entire tube length. As shown in Fig. 10, however, the experimental total energy evaluated by this method and the numerical predictions, deviate by a maximum of 70-percent at high Fourier numbers ($Fo \geqslant 2$) and at low flow rates ($Pe = 14\,350$). Since the volume of accumulated ice is a square function of diameter, the error made in estimating the local diameter of the ice-layer by a linear extrapolation will be squared in computing the total volume at these working conditions. As the flow rate increases, however, a more uniform distribution in ice-layer diameters along the flow direction is attained and the deviation in energy predictions remains within acceptable limits of engineering accuracy.

After demonstrating the numerical and the physical validity of the computer code, a parametric study on thermal behavior of the system has been pursued. Fig. 11 presents the time wise variation of the total thermal energy stored by the system for Peclet numbers of 28 700 (lower curves), and 143 500 (upper curves). To determine any effect of the finned tube geometry on energy storage, two extreme fin densities of 14 and 31 are considered for each flow rate and the fin diameter ratio, D_{fn}, is varied in a range between 2.0 and 5.0. It is evident that, at low flow rates, any improvement in energy storage due to exchanger geometry is hardly detectable. The high thermal resistance of heat transfer fluid surpasses the alleviation obtained by the denser fins at low flow rates. However, at high flow rates, a considerable difference in the slope of Q-curves takes place. Both the number of fins and the fin diameter play an important role on enhancing the solidification rate.

For efficient solidification/fusion processes around the tubes of ice-banks, the finned tubes are immersed in PCM with a radial distance sufficient to avoid overlapping of interfaces. Hence, each finned tube functions individually and determination of the amount of energy stored per meter of each tube has a practical significance. The present apparatus provides such experimental results and Fig. 12 shows thermal energy storage capacity of the finned tube exchanger for cases; $Ste = 0.19$, $D_{\mathrm{fn}} = 3.2$, and fin densities at 0, 14, 23, and 31. In accord with the numerical findings, this figure indicates that the effect of fin density on energy storage is only distinguished at high flow rates; $Pe \geqslant 86\,100$. The enhancement in energy storage due to surface geometry may be justified by comparing the time-wise averaged energy values. Fig. 12 indicates that for flow conditions; $Pe = 143\,500$, $Ste = 0.19$, and for $D_{\mathrm{fn}} = 3.2$, doubling the fin density in-

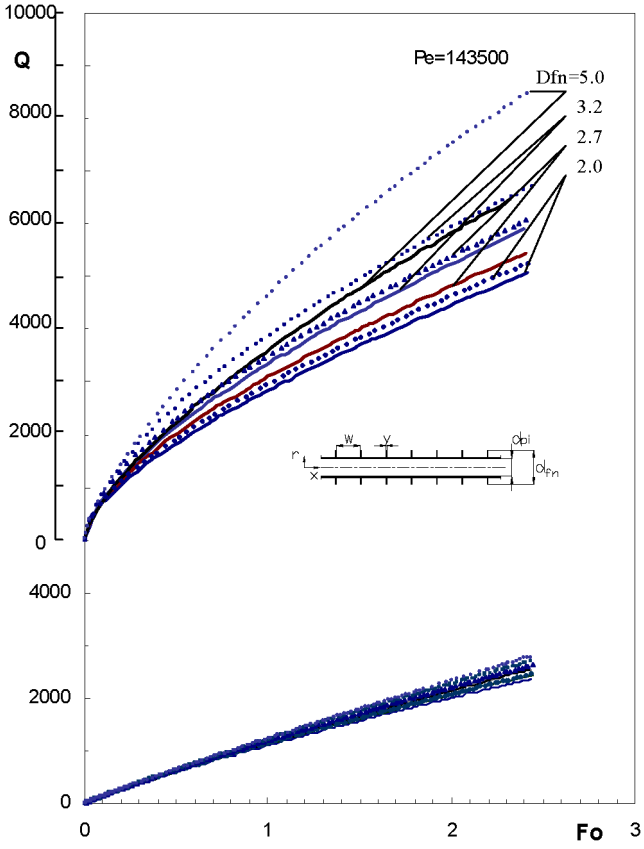

Fig. 11. Computed results of total cold thermal energy stored by the exchanger for tests at $Ste = 0.19$ with the fin density; $N_{fn} = 14$ (lines), and 31 (symbols).

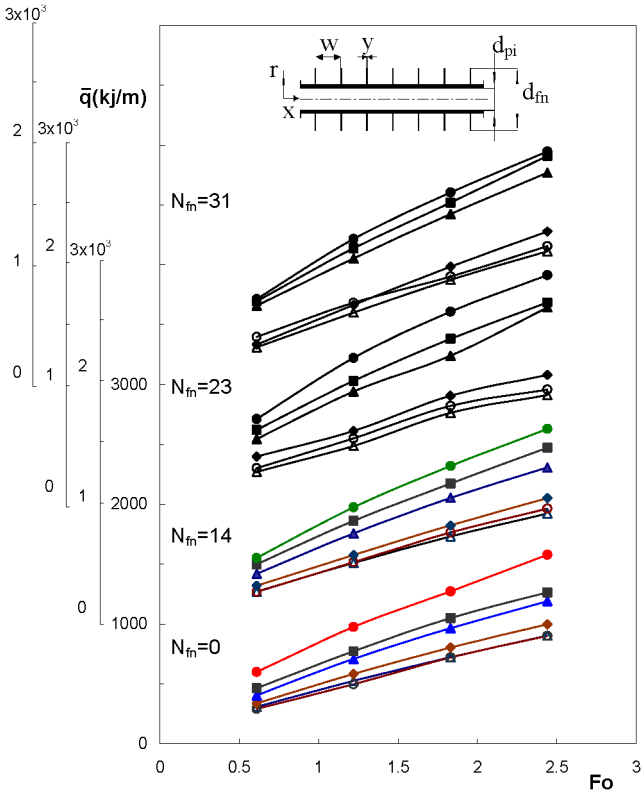

Fig. 12. Experimental results on total energy stored per meter of the exchanger surface geometry for tests at $Ste = 0.19$, $D_{fn} = 3.2$, and Peclet numbers: (△, 14 350; ○, 28 700; ◆, 57 400; ▲, 86 100; ■, 143 500; ●, 200 900).

creases the mean value of the energy storage (averaged over a region; $0.61 \leqslant Fo \leqslant 2.44$) by 30-percent. In addition, this figure supplies data for the bare tube case ($N_{fn} = 0$) and may assist determining the improvement in thermal performance due to fins. For instance, the finned tube surface defined as: $N_{fn} = 31$, $D_{fn} = 3.2$, stores 45-percent as more energy as stored by a bare tube in time-wise average basis at flow conditions of $Pe = 143\,500$, and $Ste = 0.19$.

6. Concluding remarks

A numerical code has been developed for the analysis of ice formation on a horizontal finned tube having a finite tube wall and fin thicknesses. Stable and accurate results are generated using fully implicit scheme in the axial and the radial directions and in time. The code enables all the information necessary to be obtained in studying the energy storage in ice-banks, for which conduction is prevalent over the other heat transfer effects. To test the physical validity of the code results, an experimental apparatus has been designed and built by which the effect of the heat transfer fluid inlet temperature, the flow rate, the fin density, and the fin size on cold thermal energy storage can be studied.

Including the bare tube, a total of seven tube configurations is experimentally tested and numerically studied. The flow rate of HTF is varied in range so that the flow Reynolds number covered the laminar and the turbulent flow regimes and assumed values between 500 and 7000. Comparisons between experimental and numerical distributions of phase fronts and surface temperatures give very good results. In these comparisons, only minor discrepancies arise. In addition to the instrumental uncertainty, when it is considered that in the experiments the heat transfer through the side walls of the test section is small but not negligible, the results of comparison serve to justify the assumptions made as the basis of the mathematical model.

The analysis in energy storage of the system indicate that dimensionless value of the total energy stored increases for increasing the Fourier number and also for increasing the Stefan number. Within the range of the fin density ($14 \leqslant N_{fn} \leqslant 31$) and the size ($2.7 \leqslant D_{fn} \leqslant 3.2$) studied, no appreciable change in the amount of energy stored is observed for laminar flow of the HTF ($Re < 2300$). In turbulent flow regime, however, the presence of long and denser fins significantly accelerates the solidification process and a jump in the stored energy takes place. In fact, it has been demonstrated experimentally that for identical flow and inlet conditions, the heat exchanger with $N_{fn} = 31$ fins·m^{-1}, and $D_{fn} = 3.2$

stores as high as 45-percent more energy than the bare tube in turbulent flow regime ($Re > 3000$).

Acknowledgement

The authors would like to acknowledge the financial assistance provided by the University Research Funds under the Grant No. 03.kb.fen.025.

References

[1] Thermal storage, HVAC applications, in: ASHRAE Handbook, 1999 (Chapter 46).
[2] B. Zalba, J.M. Marin, L.F. Cabeza, H. Mehling, Review on thermal energy storage with phase change: materials, heat transfer analysis, and applications, Appl. Thermal Engrg. 23 (2003) 251–283.
[3] A. Saito, Recent advances in research on cold thermal energy storage, Internat. J. Refrig. 25 (2002) 177–189.
[4] M. Lacroix, Study of the heat transfer behavior of a latent heat thermal energy storage unit with a finned tube, Internat. J. Heat Mass Transfer 36 (8) (1993) 2083–2092.
[5] W.M. Kays, M.E. Crawford, Convective Heat and Mass Transfer, second ed., McGraw-Hill, New York, 1980 (Chapter 8).
[6] Y. Zhang, A. Faghri, Heat transfer enhancement in latent heat thermal energy storage system by using the internally finned tube, Internat. J. Heat Mass Transfer 39 (15) (1996) 3165–3173.
[7] Y. Zhang, A. Faghri, Heat transfer enhancement in latent heat thermal energy storage system by using an external radial finned tube, J. Enhanced Heat Transfer 3 (2) (1996) 119–127.
[8] M. Lacroix, M. Benmadda, Numerical simulation of natural convection dominated melting and solidification from a finned vertical wall, Numer. Heat Transfer Part A 31 (1997) 71–86.
[9] K.A.R. Ismail, J.R. Henriquez, L.F.M. Moura, M.M. Ganzarolli, Ice formation around isothermal radial finned tubes, Energy Convers. Management 41 (2000) 585–605.
[10] American Society for Metals, Properties and Selection: Nonferrous Alloys and Special Purpose Materials, tenth ed., ASM Handbook, vol. 2, ASM, Metals Park, OH, 1998, pp. 305–376.
[11] R.H. Perry, D. Green, Perry's Chemical Engineer's Handbook, sixth ed., McGraw-Hill, New York, 1984 (Section 3).
[12] R.C. Gonzales, R.E. Woods, Digital Image Processing, second ed., Addison-Wesley, 2002 (Chapter 6).
[13] S.J. Kline, F.A. McClintock, Describing uncertainties in single sample experiments, Mech. Engrg. 75 (1) (1953) 3–8.
[14] V. Gnielinski, New equations for heat and mass transfer in turbulent pipe and channel flow, Internat. Chem. Engrg. 16 (1976) 359–368.
[15] E.M. Sparrow, J.W. Ramsey, J.S. Harris, The transition from natural-convection-controlled freezing to conduction-controlled freezing, J. Heat Transfer 103 (1981) 7–12.
[16] H.K. Versteeg, W. Malalasekera, An Introduction to Computational Fluid Dynamics—The Finite Volume Method, Prentice-Hall, Englewood Cliffs, NJ, 1995.
[17] S.L. Lee, A strongly implicit solver for two-dimensional elliptic differential equations, Numer. Heat Transfer Part B 16 (1989) 161–178.